登録日：2011年4月8日
US 7888891（米国）
登録日：2011年2月15日

8) PET撮像による画像定量化装置、方法、プログラム及び該画像定量化プログラムを記録したコンピュータ読み出し可能な記録媒体
特許第4701406号
登録日：2011年3月18日

9) 断層撮影画像の重ね合わせ方法及び断層撮影画像を重ね合わせて表示するためのコンピュータプログラム
出願日：2006年9月28日
出願番号：2007-537664

10) 断層撮影装置
特許第4929448号
登録日：2012年2月24日

11) 実験動物固定装置
出願日：2007年4月24日
公開番号：2009-213373

12) 脳画像化装置用頭部模型及びその製造技術
出願日：2009年4月10日
出願番号：2009-96188
PCT：2010年4月6日出願／JP2010/056196

13) 標識化合物供給システム
出願日：2009年8月19日
公開番号：2011-043356

2.実用新案登録
なし

3.その他
なし

資料 1

Rapid quantitative CBF and $CMRO_2$ measurements from a single PET scan with sequential administration of dual ^{15}O-labeled tracers

Nobuyuki KUDOMI[1,2], Yoshiyuki HIRANO[1], Kazuhiro KOSHINO[1], Takuya HAYASHI[1,*], Hiroshi WATABE[1,**], Kazuhito FUKUSHIMA[3], Hiroshi MOROIWAKI[4], Noboru TERAMOTO[1,**] and Hidehiro IIDA[1]

[1]*Department of Investigative Radiology, National Cerebral and Cardiovascular Center, Research Institute, 5-7-1, Fujishirodai, Suita, Osaka, 565-8565, Japan;* [2]*Department of Medical Physics, Faculty of Medicine, Kagawa University, 1750-1 Ikenobe, Miki, Kitagun, Kagawa, 761-0793, Japan;* [3]*Department of Radiology, National Cerebral and Cardiovascular Center, 5-7-1, Fujishirodai, Suita, Osaka, 565-8565, Japan;* [4]*Division of Neurology, Department of Cerebrovascular Diseases, National Cerebral and Cardiovascular Center, 5-7-1, Fujishirodai, Suita, Osaka, 565-8565, Japan.*

PET with ^{15}O-tracers provides essential information in patients with cerebral vascular disorders. Dual-tracer autoradiography (DARG) is a method of quantitatively assessing cerebral blood flow (CBF), oxygen extraction fraction (OEF), and metabolic rate of oxygen ($CMRO_2$) from a short, single dynamic PET scan in conjunction with sequential administration of $^{15}O_2$ and $H_2{}^{15}O$. DARG, however, requires an additional $C^{15}O$-PET scan to measure cerebral blood volume (CBV). We aimed to remove the CBV scan and calculate all functional images only from a single dynamic PET scan, thus shortening the entire examination period <10 min.

The technique was based on the dual-tracer approach with a basis function method (DBFM). Validity was tested on 6 monkeys by comparing global OEF derived by PET with those obtained by arteriovenous blood sampling, and tested clinical feasibility on normal subjects.

The mean DBFM-derived global OEF was 0.57±0.06 in monkeys, in an agreement with that by the arteriovenous method (0.54±0.06). Image quality was similar and differences from DARG were 0.020 to 0.024 mL/min/g for CBF, and –0.0006 to –0.0033 mL/min/g for $CMRO_2$. A simulation study demonstrated similar error propagation between DBFM and DARG.

The DBFM method enables rapid and accurate assessment of CBF and $CMRO_2$ in clinical settings.

Key words: positron emission tomography, cerebral blood flow, kinetic modeling, acute stroke, and brain imaging

Introduction

Quantitative cerebral blood flow (CBF), oxygen extraction fraction (OEF) and metabolic rate of oxygen ($CMRO_2$) images can be assessed using positron emission tomography (PET) and ^{15}O-labeled radiotracers. These parametric images are essential for understanding the pathophysiological status of cerebral vascular disorders, and this technique has been promoted as a clinical diagnostic tool. Parametric images have been measured via PET by administering multiple ^{15}O-labeled tracers (Frackowiack *et al*, 1980; Mintun *et al*, 1984), such as in the steady-state method (Subramanyam *et al*, 1978; Lammertsma *et al*, 1982) or the 3-step autoradiography method (Mintun *et al*, 1984; Hatazawa *et al*, 1995). The validity of the technique has been demonstrated with 3-step autoradiography on healthy volunteers at rest (Hattori *et al*, 2004). More than one hour, however, is typically required to complete the whole study, because 3 independent scans are required in addition to >10-min intervals between scans to allow for decay of the residual radioactivity of the preceding tracer. Thus, applicability is limited in clinical settings,

particularly for patients with acute stroke (Shimosegawa *et al*, 2005).

We recently developed a novel PET protocol involving the computational methodology of dual-tracer autoradiography (DARG), which allows for shortened examination times (Kudomi *et al*, 2005). The rapid DARG method is based on a single PET scan with sequential administration of dual tracers, and the DARG technique has demonstrated OEF values in good agreement with those assessed by the arteriovenous oxygen difference in monkeys over a wide physiological range (Kudomi *et al*, 2005), suggesting the validity of this approach. The DARG technique does, however, require additional CBV data from a $C^{15}O$ scan to compensate for radioactivity from the vascular space.

In the present study, we developed a formula that eliminates the need for the CBV information previously required by the DARG approach. This computational refinement, namely, dual-tracer basis function method (DBFM), enables the duration of the total clinical examination to be shortened significantly, to less than 10 min. The validity of the present method, in terms of quantitative accuracy and quality of generated images, was tested in anaesthetized monkeys and in normal human subjects.

Theory

The present formula was developed to compute CBF, $CMRO_2$, and CBV simultaneously while eliminating the need for a CBV image. The distributions of tracer in the vascular space (V_A^W (mL/g) for water and V_0^O (mL/g) for oxygen components) were estimated from dynamic image data acquired during sequential administration of $H_2{}^{15}O$ and $^{15}O_2$. The kinetics for both $^{15}O_2$ and $H_2{}^{15}O$ are expressed using the single-tissue compartment model (Mintun *et al*, 1984) as:

$$Ci(t) = E \cdot f \cdot A_o(t) \otimes e^{-\frac{f}{p}t} + f \cdot A_w(t) \otimes e^{-\frac{f}{p}t} + V_0^o \cdot A_o(t) + V_A^w \cdot A_w(t) \quad (1)$$

ty concentration in a voxel in a tissue region, $A_o(t)$ (Bq/mL) and $A_w(t)$ (Bq/mL) are the arterial input functions of oxygen and water contents, respectively, f (mL/min/g) is the CBF, E is the OEF, p (mL/g) is the blood/brain partition coefficient for water, and $\otimes$ indicates the convolution integral. The first and second terms on the right side represent the tissue radioactivity of oxygen and water, respectively. The last 2 signify the radioactivity of $^{15}O_2$ and $H_2{}^{15}O$ in blood vessels. In this study, p was fixed at 0.8 mL/g (Iida *et al*, 1991).

The first 2 terms on the right side in Eq (1) are nonlinear against f, and we formed basis functions to calculate parametric images for dynamic data, i.e., we applied the basis function method (Keoppe *et al*, 1985). The corresponding basis functions were as follows:

$$\begin{aligned} F_1(f,t) &= f \cdot A_w \otimes e^{-\frac{f}{p}t} \\ F_2(f,t) &= f \cdot A_o \otimes e^{-\frac{f}{p}t} \end{aligned} \quad (2)$$

Eq. (1) can then be transformed for each basis function into a linear equation in E, V_0^O, and V_A^W as:

$$Ci(t) = F_1 + E \cdot F_2 + V_0^o \cdot A_o + V_A^w \cdot A_w \quad (3)$$

For fixed values of f, then, E, V_0^O, and V_A^W could be estimated using standard linear least squares. The f for which the residual sum of squares is minimized is determined by a direct search, and associated parameter values for this solution (f, E, V_0^O, V_A^W) are obtained. For the physiologically reasonable range of f, i.e., $0 < f < 2.0$ mL/min/g, 200 discrete values for f were found to be sufficient, and CBF (f) and OEF (E) as well as V_0^O and V_A^W were obtained. $CMRO_2$ is then calculated from the obtained f, E, and the arterial oxygen concentration. The present formula can be applied to either of 2 procedures: $H_2{}^{15}O$ injection (or $C^{15}O_2$ inhalation) followed by $^{15}O_2$ inhalation ($H_2{}^{15}O$-$^{15}O_2$), or $^{15}O_2$ inhalation followed by $H_2{}^{15}O$ injection (or $C^{15}O_2$ inhalation) ($^{15}O_2$-$H_2{}^{15}O$).

Materials and Methods

The validity of the present method was tested in anaesthetized monkeys by comparing the global OEF values obtained using this approach to those derived using the arteriovenous difference method (A-V difference). We compared the regional

values of CBF and $CMRO_2$ for normal human subjects derived by the present DBFM and the DARG methods. The error sensitivity of the present method was tested by simulation studies.

Subjects

The present experimental study consisted of 2 groups, namely, 6 normal monkeys under anaesthesia (*macaca fascicularris*) and 7 normal human subjects.

All monkeys were males with a mean body weight of 5.2 ± 0.8 kg and ages ranging from 3 to 4 years. Animals were maintained and handled in accordance with the Human Care and Use of Laboratory Animals guidelines (Rockville, National Institute of Health/Office for Protection from Research Risks, 1996). The study protocol followed the Guidelines for Animal Experimentation of the National Cerebral and Cardiovascular Center.

All normal human subjects were males with a mean age of 25.3 ± 2.4 years and mean body weight of 64.2 ± 6.8 kg. None had symptoms at the time of PET examination, or histories of cerebral or other relevant diseases. All subjects gave written informed consent, approved by the ethics committee of the National Cerebral and Cardiovascular Center.

PET Experiments

Details regarding the primate animal study have been previously reported (Kudomi *et al*, 2005). Briefly, anaesthesia was induced with ketamine and maintained during the experiment using intravenous propofol and vecuronium. Animals were intubated and their respiration was controlled by an anaesthetic ventilator (Cato; Drager, Germany). The PET scanner used was the ECAT HR (Siemens-CTI, Knoxville, TN, USA), installed in the animal PET laboratory of the National Cerebral and Cardiovascular Research Center. PET scanning was performed in 2-D mode. After a 900-s transmission scan, a dynamic scan was started following the inhalation of $C^{15}O$. After 10 min, a 6-min dynamic PET scan was performed during sequential administration of $^{15}O_2$ (2200 MBq) and $H_2{}^{15}O$ (370 MBq) for 3 min each. After 10 min, another order of scan, namely, $H_2{}^{15}O$ followed by $^{15}O_2$ administration scan was performed. The administration order, either $H_2{}^{15}O$-$^{15}O_2$ or $^{15}O_2$-$H_2{}^{15}O$, was randomized across subjects. Arterial blood was withdrawn continuously from the femoral artery and the blood radioactivity concentration was measured with a continuous input function monitor system made of GSO scintillation crystals (Kudomi *et al*, 2003). Arterial and sinus blood samples of 0.2 mL each were drawn simultaneously during each scan. Their oxygen contents were measured to obtain the global OEF ($gOEF_{A\text{-}V}$) (Kudomi *et al*, 2005).

In 3 of the 6 animals, A-V sampling and the PET scan using the $^{15}O_2$-$H_2{}^{15}O$ administration order were performed simultaneously not only during normocapnia ($PaCO_2 \cong 40$ mmHg) but also while the respiratory rate was sequentially adjusted to yield hypocapnia ($PaCO_2 < 33$ mmHg), mild hypercapnia ($45 < PaCO_2 < 50$ mmHg), and deep hypercapnia ($PaCO_2 > 50$ mmHg). At least 30 min were allotted to reach a steady-state P_aCO_2, after which a $^{15}O_2$-$H_2{}^{15}O$ PET scan was performed.

Human subjects were studied at the Radiology Department of the National Cerebral and Cardiovascular Research Center. Young, healthy volunteer subjects were scanned with an ECAT 47 scanner (Siemens-CTI, Knoxville, TN, USA). The scanning was carried out in 2-D mode. After a transmission scan, a static scan was started 2 min following the 4-min inhalation of 3000 MBq of $C^{15}O$. After a pause of 10 min to permit radioactive decay, 2 sets of dynamic scans of 540 s and 510 s were carried out, first during sequential inhlation of $C^{15}O_2$ (3000 MBq) and $^{15}O_2$ (4500 MBq), and second an inhalation of $^{15}O_2$ (4500 MBq) followed by intravenous $H_2{}^{15}O$ (1100 MBq), respectively. Since the ^{15}O label in $C^{15}O_2$ is rapidly transferred to the water pool in the lung capillary bed (West and Dollery, 1962), the $C^{15}O_2$ inhalation is considered essentially identical to the intravenous administration of $H_2{}^{15}O$. Thus, $C^{15}O_2$ - $^{15}O_2$ procedure is noted as $H_2{}^{15}O$-$^{15}O_2$ protocol in this article.

Arterial blood was continuously drawn from the brachial artery using a catheter and syringe pump (Harvard Apparatus, model 901) at a speed of 2.0 mL/min during the PET scan, and the blood radioactivity concentration was measured using

the GSO input function monitor system (Kudomi *et al*, 2003).

Data Processing

Dynamic sinogram data were corrected for dead time in each frame and for detector normalization. Tomographic images were reconstructed using the filtered back projection method with 4- and 7-mm Gaussian filtering for monkeys and human subjects, respectively. Attenuation correction was applied using transmission data. Scatter correction was also applied by means of the deconvolution scatter function technique (Shao *et al*, 1991). Reconstructed images, with a matrix size of 128 × 128 × 47 and a voxel size of 1.1 mm × 1.1 mm × 3.4 mm for monkeys and 1.8 mm × 1.8 mm × 3.4 mm for normal human subjects, were transferred to a LINUX computer for further analysis using in-house programs.

Measured arterial blood time activity curves (TAC) were also corrected for dispersion (τ = 3 s and 14 s for monkeys and humans, respectively) (Iida *et al*, 1986). After correcting for delay (Iida *et al*, 1988; Kudomi *et al*, 2005), the blood curves were separated into $^{15}O_2$ (A_O) and $H_2{}^{15}O$ (A_W) contents as described previously (Kudomi *et al*, 2007, 2009), and input functions were obtained.

Functional CBF, OEF, and $CMRO_2$ images were calculated according to the DBFM formula described above, using reconstructed images and the obtained input functions. Corresponding images were also generated using the DARG formula (Kudomi *et al*, 2005). With DBFM, blood volume was estimated as $V_0{}^O$, and the obtained images were converted to CBV images using the following: $V_0{}^O = V_B/R_{Hct}\ (1–E{\cdot}F_v)$, where R_{Hct} is the small-to-large vessel hematocrit ratio and F_v is the effective venous fraction (Mintun *et al*, 2004). For both DBFM and DARG, the set of images was generated without applying physical decay correction.

Data Analysis

Regions of interest (ROIs) were drawn on CBF images obtained from monkeys to cover the whole brain. These ROIs were then transferred to the OEF and $CMRO_2$ functional images obtained using the DBFM and DARG methods. Quantitative CBF, OEF, and $CMRO_2$ values generated from DBFM were then compared with those from DARG. Also, OEF values obtained from DBFM were compared with those using the A-V sampling technique ($OEF_{A\text{-}V}$).

In normal subjects, circular ROIs of 6-mm diameter were placed bilaterally on the temporal, frontal, parietal, occipital, and cerebellar, brain stem, caudate, lentiform, thalamus, and central semioval regions. Values for CBF, and $CMRO_2$ in the same ROIs were summarized for the cortical grey matter, deep grey matter, cerebellum and white matter regions, and were compared between DBFM and DARG using Bland-Altman plots.

The *N*-index, which denotes the noise level of parametric images (Kudomi *et al*, 2010), was obtained from the standard deviation of an image's spatial values, which was derived by subtracting 2 statistically independent and physiologically equivalent images. This calculation was carried out for CBF, OEF, and $CMRO_2$ from normal human subjects using even- and odd-numbered frames, and the obtained *N*-index values were compared between the DARG and DBFM formulae.

All data are presented as means ± 1 SD. Pearson's correlation analysis and linear regression analysis were used to evaluate relationships between the 2 CBF values. $P < 0.05$ was considered statistically significant.

Simulation

Error propagation was evaluated for 3 error sources, namely: effects of the imperfect delay adjustment (Iida *et al*, 1988), by shifting time in an input function from –4 to 4 s, where a positive error represents an overcorrection of delay time; errors in dispersion correction in the input function (Iida *et al*, 1986), by shifting the time constant from –4 to 4 s, where a negative error represents undercorrection, as described previously (Iida *et al*, 2000; Kudomi *et al*, 2005); and errors in the assumed blood/tissue partition coefficient (p) (Iida *et al*, 1991; Kudomi *et al*, 2005), by varying *p* from 0.7 to 0.9 mL/g (Iida *et al*, 1991).

The input function for this simulation study was defined based on typical arterial time-activity curves (TACs) obtained from a human study with

water (*Aw*) and also with oxygen (*Ao*) (Shidahara *et al*, 2001), and by adding the *Aw* and *Ao* with a time lag of 3 min between the administrations of $H_2{}^{15}O$-$^{15}O_2$ and $^{15}O_2$- $H_2{}^{15}O$. Applying the kinetic formulation of Eq. (1), tissue TACs were generated for "normal" (CBF = 50 mL/100 g/min^{-1}, OEF = 0.4, and CBV = 0.04 mL/g), and "ischemic" (decreased CBF with enhanced OEF) (CBF = 30 mL/100 g/min, OEF = 0.6, and CBV = 0.04 mL/g) conditions (Kudomi *et al*, 2005).

Values of CBF, OEF, and $CMRO_2$ were then calculated using the true input function and these TACs, assuming p = 0.8 mL/g. Errors in these calculated values were presented as a function of the percentage differences from the assumed values for delay, dispersion, and the partition coefficient.

Results

Quantitative values for whole brain in monkeys were 32 ± 11 and 27 ± 9 ml/100g/min in CBF for DARG and DBFM, respectively, 0.56 ± 0.06 and 0.57 ± 0.06 in OEF for DARG and DBFM, respectively, and 2.9 ± 0.4 and 2.6 ± 0.4 ml/100g/min in $CMRO_2$ for DARG and DBFM, respectively. The OEF value by the A-V method was 0.54 ± 0.06. The paired *t*-test did not show any significant differences in these values between DARG and DBFM for either order, i.e., $H_2{}^{15}O$-$^{15}O_2$ and $^{15}O_2$-$H_2{}^{15}O$ ($P > 0.05$, $n = 6$). Also, there were no significant differences in OEF between the PET and the A-V methods, for either order ($p > 0.05$, $n = 6$). During normocapnia, the P_aCO_2, P_aO_2, S_aO_2, and hemoglobin values were 38.9 ± 1.4 mmHg, 119 ± 12 mmHg, 97.3 ± 1.2 %, and 13.6 ± 1.0 g/dL, respectively; all of these are considered to be within the normal range.

Figure 1 shows the DBFM-derived OEF values plotted against the $OEF_{A\text{-}V}$ values obtained during P_aCO_2 variation. The regression line obtained was: $OEF = 0.99\ OEF_{A\text{-}V} - 0.01$ ($r = 0.96$, $p < 0.001$, $n = 12$). The intercept was not significantly different from zero ($P > 0.05$), and the slope of the line was close to unity.

The Bland-Altman plots of regional ROI values of CBF and $CMRO_2$ as estimated by DARG and DBFM for normal human subjects are shown in Figure 2. The plots demonstrate small overestimation by the DBFM method, with biases of 0.024 and 0.021 mL/min/g for CBF by H_2O-O_2 and O_2-H_2O, respectively, and underestimation of –0.0006 and –0.0033 mL/min/g for $CMRO_2$ by H_2O-O_2 and O_2-H_2O, respectively. The paired *t*-test showed no significant difference between the methods in terms of CBF for either order, or for $CMRO_2$ with $H_2{}^{15}O$-$^{15}O_2$. For CBV, the differences were 0.002 ± 0.022 and 0.021 ± 0.019 g/mL for H_2O-O_2 and O_2-H_2O, respectively. The mean and SD values for these parametric values are summarized in Table I.

Figure 3 provides a representative set of CBF, OEF, and $CMRO_2$ images generated by DBFM and DARG for a normal subject. The parametric images generated by DBFM were of comparable quality to those obtained using DARG. The CBV images obtained by CO scanning as well as the H_2O-O_2 and O_2-H_2O methods are shown in Figure 4. The images from the DBFM methods show a similar distribution to those produced using the CO scan methods, but the quality in these images suffer from noise.

A comparison of image quality is given in Figure 5. The quality is measured by dividing the *N*-index by the mean value of each of CBF, OEF, and $CMRO_2$. For CBF, the means of *N*-index/mean/ $\sqrt{2}$ for $H_2{}^{15}O$-$^{15}O_2$ were 0.098 ± 0.021 and 0.108 ± 0.020 for DARG and DBFM, respectively, and those for $^{15}O_2$-$H_2{}^{15}O$ were 0.102 ± 0.012 and 0.120 ± 0.012 for DARG and DBFM, respectively. For OEF, the values for $H_2{}^{15}O$-$^{15}O_2$ were 0.109 ± 0.015 and 0.153 ± 0.018 for DARG and DBFM, respectively, and those for $^{15}O_2$-$H_2{}^{15}O$ were 0.114 ± 0.012 and 0.150 ± 0.023 for DARG and DBFM, respectively. For $CMRO_2$, the values for $H_2{}^{15}O$-$^{15}O_2$ were 0.116 ± 0.025 and 0.136 ± 0.029 for DARG and DBFM, respectively, and those for $^{15}O_2$-$H_2{}^{15}O$ were 0.101 ± 0.013 and 0.132 ± 0.022 for DARG and DBFM, respectively. Small increases in noise were observed with DBFM compared to DARG.

Results of the simulation are shown in Figure 6. Error sensitivity to errors in delay time, the dispersion time constant, and the partition coefficient value were not significantly higher for DBFM than for DARG.

In the CBF-decreased and OEF-elevated condition, the magnitude of error in the functional

values was roughly the same in terms of delay and dispersion. The magnitude was relatively smaller in terms of p; namely, relative to normal tissue, the magnitude for CBF was 50% for H_2O-O_2 and 70% for O_2-H_2O; for OEF the magnitude was 50% for H_2O-O_2 and 30% for O_2-H_2O; and for $CMRO_2$ the magnitude was 50% for H_2O-O_2 and 50% for O_2-H_2O.

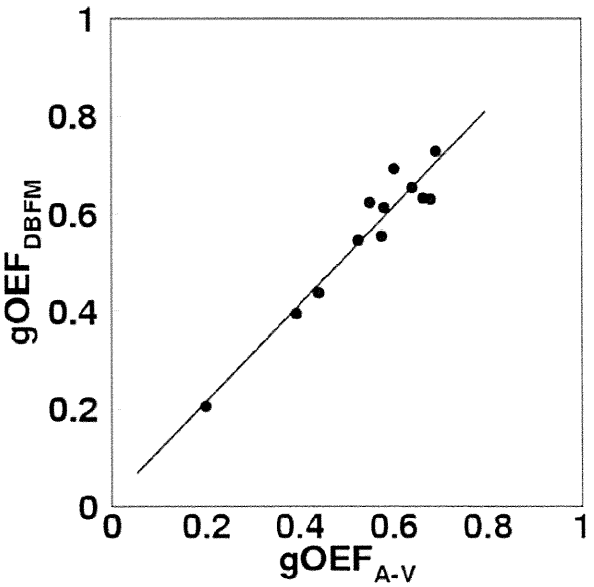

Figure 1. Plots of OEF measured using arteriovenous difference (gOEF(A-V)) and DBFM (gOEF(PET)). The regression analysis exhibited a significant positive correlation with a slope close to unity (y = 0.99 x + 0.01, r = 0.96, *number of plots* = 12). DBFM was performed with an administration order of O_2-H_2O. DBFM: dual tracer basis function method

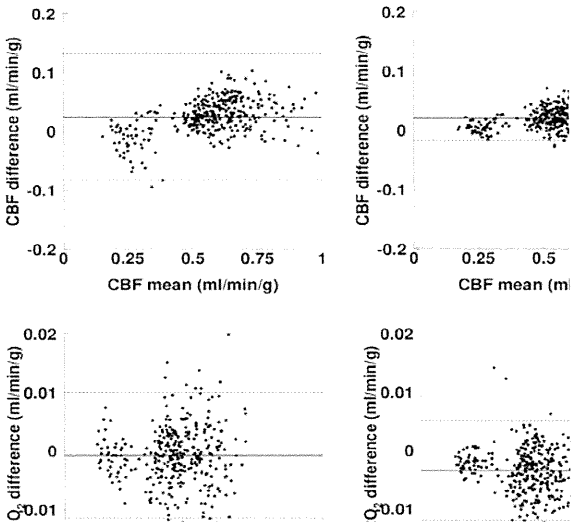

Figure 2. Bland-Altman plots of CBF (upper) and $CMRO_2$ (lower) for H_2O-O_2 (left) and O_2-H_2O (right) comparing DARG and DBFM regional values in normal subjects. Solid and broken lines show mean difference and its respective 2SD, respectively. Means ± SD values are 0.024 ± 0.030 mL/min/g for CBF by H_2O-O_2, 0.021 ± 0.019 mL/min/g for CBF by O_2-H_2O, –0.000685 ± 0.00536 mL/min/g for $CMRO_2$ by H_2O-O_2, and –0.00339 ± 0.00426 mL/min/g for $CMRO_2$ by O_2-H_2O.

TABLE I. CBF, OEF and $CMRO_2$ values in normal human subjects (n = 7) in cortical grey matter, deep grey matter, cerebellum and white matter regions calculated using DARG and DBFM

		DARG		DBFM	
		$H_2{}^{15}O$-$^{15}O_2$	$^{15}O_2$-$H_2{}^{15}O$	$H_2{}^{15}O$-$^{15}O_2$	$^{15}O_2$-$H_2{}^{15}O$
CBF (mL/100 g/min)	Cortical Grey	52.5 ± 4.1	50.7 ± 4.1	52.5 ± 4.6	52.1 ± 4.1
	Deep Grey	54.2 ± 4.3	53.1 ± 3.8	57.2 ± 6.0	54.5 ± 3.8
	Cerebellum	58.2 ± 10.6	55.2 ± 5.1	59.1 ± 10.3	55.7 ± 5.3
	White matter	27.8 ± 4.5	26.7 ± 3.6	26.0 ± 5.0	26.0 ± 3.4
OEF	Cortical Grey	0.39 ± 0.05	0.41 ± 0.03	0.39 ± 0.06	0.39 ± 0.03
	Deep Grey	0.43± 0.05	0.43 ± 0.05	0.38 ± 0.05	0.40 ± 0.05
	cerebellum	0.36 ± 0.04	0.41 ± 0.07	0.38 ± 0.05	0.40 ± 0.06
	White	0.37 ± 0.05	0.40 ± 0.03	0.38 ± 0.06	0.39 ± 0.03
$CMRO_2$ (mL/100 g/min)	Cortical Grey	4.21 ± 0.68	4.27 ± 0.49	4.21 ± 0.71	4.15 ± 0.44*
	Deep Grey	4.78 ± 0.70	4.69 ± 0.71	4.50 ± 0.75	4.52 ± 0.63*
	cerebellum	4.31 ± 0.89	4.64 ± 0.88	4.62 ± 0.88	4.51 ± 0.73*
	White	2.12 ± 0.56	2.19 ± 0.49	2.05 ± 0.43	2.08 ± 0.42
CBV (g/100 mL)	Cortical Grey	4.44 ± 0.88		4.10 ± 0.78	5.90 ± 1.02*
	Deep Grey	4.96 ± 1.02		4.99 ± 1.06	7.05 ± 1.06*
	cerebellum	6.44 ± 0.38		3.60 ± 2.01*	5.86 ± 2.20*
	White	1.88 ± 0.44		2.59 ± 0.92*	3.72 ± 0.60*

(n = 7; values are presented as Means ± SD; DARG: dual-tracer autoradiography; DBFM: dual-tracer basis function method; *: difference was significant between DARG and DBFM)

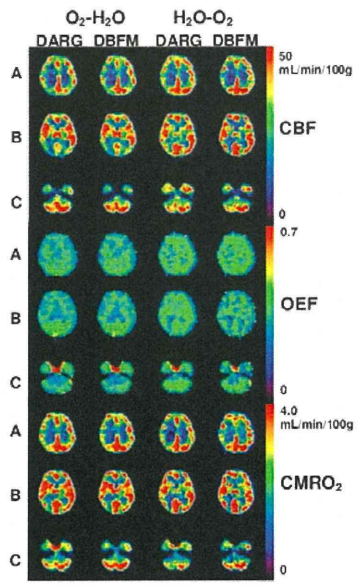

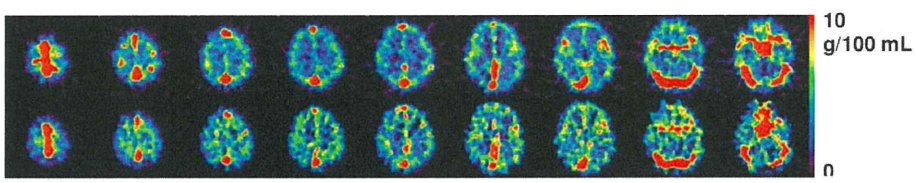

Figure 3. Representative view of CBF, OEF, and $CMRO_2$ images for a normal subject using DARG and DBFM techniques with H_2O-O_2 and O_2-H_2O modes. Axial images are sectioned at (A) parietal level, (B) basal ganglia level, and (C) cerebellar level.

Figure 4. Representative view of CBV images in a normal subject, derived by CO scan (upper) and DBFM (O_2-H_2O) (lower) methods.

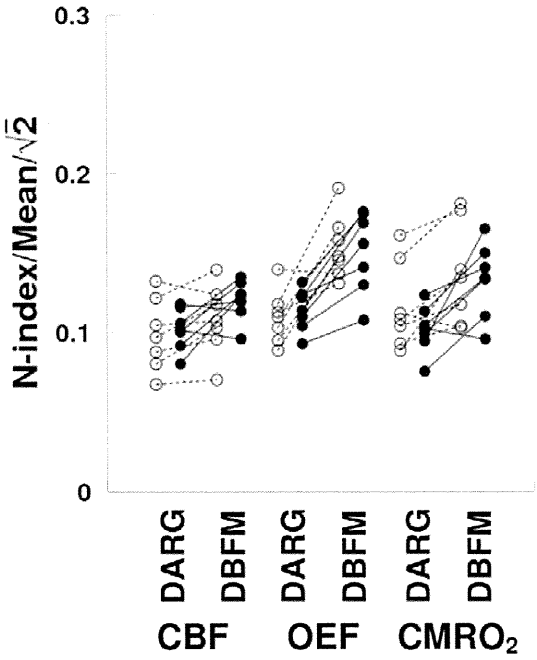

Figure 5. Comparison of noise levels between DARG and DBFM for CBF, OEF, and $CMRO_2$ images by means of *N*-index.

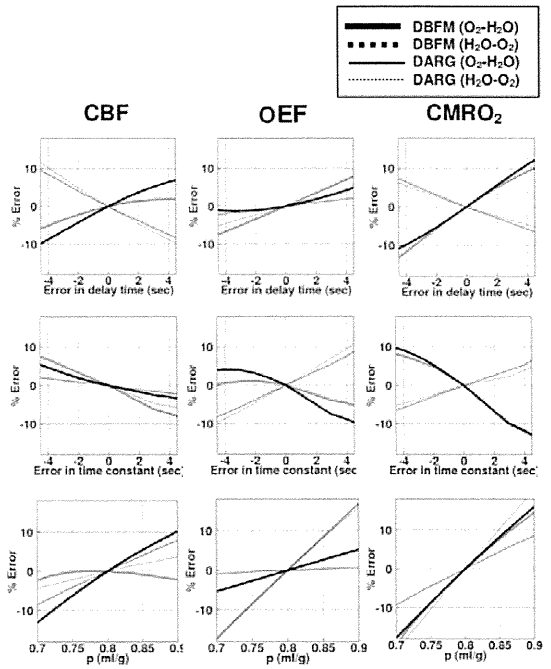

Figure 6. Error propagation from the errors in input delay time (upper) and the dispersion time constant (middle), and from the partition coefficient (*p* mL/g) (lower) to CBF, OEF, and $CMRO_2$. Positive and negative values of errors in delay time indicate over- and under-correction of delay time, respectively. Positive and negative values of errors in the time constant indicate under- and over-correction of dispersion time, respectively. DARG: dual-tracer autoradiographic method; DBFM: dual-tracer basis function method; H_2O-O_2: H_2O followed by O_2; O_2-H_2O: O_2 followed by H_2O.

Discussion

This study successfully used the DBFM approach to derive quantitative images of CBF, $CMRO_2$, and OEF from a single, short-duration dynamic PET scan with sequential administration of $^{15}O_2$ and $H_2{}^{15}O$ or $H_2{}^{15}O$ and $^{15}O_2$ within a short time interval. Functional values obtained by the DBFM method were in good agreement with those derived by the A-V oxygen difference in the experiment utilizing 6 monkeys (Fig. 1). There was a significant difference in $CMRO_2$ between DBFM and DARG for $^{15}O_2$-$H_2{}^{15}O$ administration, but the magnitude of the differences in CBF and $CMRO_2$ for both administration orders was small (Fig. 2). Image quality for CBF, OEF, and $CMRO_2$ was found to be similar between DBFM and DARG (Fig. 3). The simulation also demonstrated that the 2 methods were almost identical in terms of quantitative error sensitivity. Since the accuracy and statistical uncertainty of DARG have already been shown by Kudomi *et al* (2005) to be identical to those of the 3-step approach of Mintun *et al* (1984), the CBF, OEF, and $CMRO_2$ values obtained by DBFM were essentially consistent with those of the 3-step technique in both clinical and research examinations.

One major improvement of DBFM over DARG is that the former does not require additional CBV assessment, and thus the entire scan period can be reduced to less than 9 min, with all 3 functional images generated in a quantitative manner. The total study duration, including patient positioning and arterial cannulation, should likely be less than 25 min in practice. This duration is considerably shorter than those of previously published techniques.

The shortening of the total scan duration significantly reduces patient exertion. This technique also extends applicability in 2 ways. First, because of drastic reduction in scan time, the approach may be used with acute stroke patients who require rapid treatment (Lees *et al*, 2010). Second, this method can be used for purposes such as investigating time variations in postembolization hemodynamic responses in animal experiment systems or analyzing the hemodynamics of a subject who received a balloon occlusion test that permitted CBF but not OEF or $CMRO_2$ assessment. We believe the present technique can be used to reveal new pathophysiological bases of cerebrovascular disorders and thus create the potential for new therapeutic strategies.

The DBFM approach eliminates the need for an additional $C^{15}O$ scan to compute CBF, OEF, and $CMRO_2$. CBV images were determined by implementing CBV in the formulation, while costly approaches such as 3-step autoradiography (Mintun *et al*, 1984; Hatazawa *et al*, 1995; Shidahara *et al*, 2002) and DARG (Kudomi *et al*, 2005) compensated the CBV by using an additional $C^{15}O$ scan and assuming a fixed fractional volume of the vein (Mintum *et al*, 1984). Although the computational procedures and assumptions differ between the present DBFM and the previous ARG and DARG approaches, the CBF, OEF, and $CMRO_2$ values obtained with these techniques were fairly consistent. In the experimental monkey study, global OEF values showed tight correlation between the present DBFM method and the A-V difference approach, with no significant difference between the 2. These findings suggest the adequacy of the DBFM technique for simultaneous assessment of CBF, OEF, and $CMRO_2$ using only a single dynamic scan.

CBV images generated by DBFM resembled those from the $C^{15}O$ inhalation scan, but with enhanced noise and systematic error. As has been previously reported (Kim *et al*, 2004), one reason for these observations is errors in the arterial input function, such as delay and dispersion. Further studies should be carried out to evaluate the adequacy of using CBV images obtained using the DBFM method as a diagnostic tool. Otherwise, an additional $C^{15}O$ inhalation scan should be acquired if one needs quantitative CBV images for reliable diagnosis.

The present simulation study revealed that for CBF, OEF, and $CMRO_2$, the error sensitivity to delay, dispersion, and assumed p differed somewhat between DBFM and DARG (Fig. 6). The error magnitudes for CBF, OEF, and $CMRO_2$ were <5% for a 2-s error in delay, 2-s error in dispersion time constant, and 5% error in p, which we thought to lie within acceptable ranges for practical use.

One primary limitation of this technique is the need for sequential radiosynthesis of 2 radioactive compounds ($^{15}O_2$ and $H_2{}^{15}O$) within a short interval. Of note is that quality control or examination of purity is also needed before administration of each radioactive compound, in order to guarantee that there is no contamination in either $^{15}O_2$ or $H_2{}^{15}O$ administrations. A cyclotron must also be operated concurrently with the study, because of the short half-life of the ^{15}O isotope. An automated synthesis system that can run under the same operating system as the ^{15}O-dedicated cyclotron may help to improve the logistics of these procedures (Miyake *et al*, 2004; Inomata *et al*, 2004). Another limitation of the technique is the need for accurate determination of the arterial input function, though this is a requirement of all techniques that quantitatively assess CBF, $CMRO_2$, and OEF. Recent improvements in the spatial resolution and extremely high counting rates of state-of-the-art PET devices may permit the non-invasive determination of the arterial input function in practical situations. Further systematic studies are warranted.

We set the time interval for sequential administration of 2 tracers to 3 min in the monkey study and 5 to 6 min in the human subject study. The time interval was longer than 3 min in the human study due to limitations in the synthesizer system. The time interval could affect the quality of the calculated CBF, OEF, and $CMRO_2$ images. A previous simulation study by Iida *et al* (2002) suggested that the quality of images calculated using DARG was identical compared to those using 3-step ARG, if the time interval was longer than 3 min. Image quality for humans was identical for DBFM and DARG (Fig. 5), suggesting that the images produced using DBFM would be acceptable for practical use.

In terms of the administration order of $^{15}O_2$ and $H_2{}^{15}O$, we confirmed that both orders provided functional parametric values consistent between the 2 protocols. In practice, however, several factors should be taken into account, such as limitations in radiosynthesis procedures, blood TAC separation into $^{15}O_2$-$H_2{}^{15}O$ components (Kudomi *et al*, 2007), image quality, quantitative accuracy, and total PET duration. The $^{15}O_2$-$H_2{}^{15}O$ scanning order is preferable, as it enables shorter scanning periods for the entire study given that the optimal scan duration is shorter for $H_2{}^{15}O$ (suggested to be 90 s by Iida *et al*, 1991) than for $^{15}O_2$ (suggested to be 180 s, Shidahara *et al*, 2002). The $H_2{}^{15}O$ may be prepared during the $^{15}O_2$ scan in this protocol.

There have been attempts to eliminate the use of CBV data for determining $CMRO_2$ by applying mathematical refinements (Meyer *et al*, 1987; Ohta *et al*, 1992); however, the quality of the calculated images suffered from statistical noise, simply because there were too many parameters (CBF, $CMRO_2$, and the vascular compartment, V_0) to be determined from just a single set of $^{15}O_2$ inhalation data. The present approach, using additional $H_2{}^{15}O$ administration, allows us to compute CBF and $CMRO_2$ parameters, and thus also OEF, with reasonable image quality and quantitative accuracy.

In conclusion, we successfully calculated CBF and $CMRO_2$ values using the formula developed in this study. The formula was applicable to PET data with sequentially administrated dual tracers and did not require the CBV data that is generally obtained from $C^{15}O$ scans. We obtained quantitatively accurate CBF and $CMRO_2$ values with reasonable image quality. We conclude that the present method is applicable to the assessment of CBF and $CMRO_2$ for both clinical and research purposes.

Dis-closure/Conflict of Interest

None of authors have conflict of interest to disclose.

Acknowledgments

The authors thank the staff of the Department of Radiology, National Cerebral and Cardiovascular Center, and Department of Investigative Radiology, National Cerebral and Cardiovascular Center-Research Institute. The present work was supported by a Grant from the Ministry of Health, Labour and Welfare (MHLW) of Japan, and also by the Program for Promotion of Fundamental Studies in Health Sciences of the Organization for Pharmaceutical Safety and Research of Japan. NK was supported by the Nakatani Electronic Measuring Technology Association of Japan, by the Ministry of Education, Science, Sports and Culture, Grant-in-Aid for Young Scientists (start-up), 21890171, 2009–2010, and by Grant-in-Aid for Scientific Research (C), 23590675, 2011–2013.

References:

Frackowiak RS, Jones T, Lenzi GL, Heather JD (1980) Regional cerebral oxygen utilization and blood flow in normal man using oxygen-15 and positron emission tomography. Acta Neurol Scand 62:336-44

Fujita H, Kuwabara H, Reutens DC, Gjedde A (1999) Oxygen consumption of cerebral cortex fails to increase during continued vibrotactile stimulation J Cereb Blood Flow Metab 19:266-71

Hatazawa J, Fujita H, Kanno I, Satoh T, Iida H, Miura S, Murakami M, Okudera T, Inugami A, Ogawa T, et al. (1995) Regional cerebral blood flow, blood volume, oxygen extraction fraction, and oxygen utilization rate in normal volunteers measured by

the autoradiographic technique and the single breath inhalation method. Ann Nucl Med. 9:15-21

Hattori N, Bergsneider M, Wu HM, Glenn TC, Vespa PM, Hovda DA, Phelps ME, Huang SC (2004) Accuracy of a method using short inhalation of ^{15}O-O_2 for measuring cerebral oxygen extraction fraction with PET in healthy humans. J Nucl Med 45: 765-770.

Iida H, Kanno I, Miura S, Murakami M, Takahashi K, Uemura K (1986) Error analysis of a quantitative cerebral blood flow measurement using $H_2{}^{15}O$ autoradiography and positron emission tomography, with respect to the dispersion of the input function. J Cereb Blood Flow Metab 6: 536-45

Iida H, Higano S, Tomura N, Shishido F, Kanno I, Miura S, Murakami M, Takahashi K, Sasaki H, Uemura K (1988) Evaluation of regional differences of tracer appearance time in cerebral tissues using [^{15}O] water and dynamic positron emission tomography. J Cereb Blood Flow Metab 8: 285-8

Iida H, Kanno I, Miura S (1991) Rapid measurement of cerebral blood flow with positron emission tomography. Ciba Found Symp 163: 23-37; discussion 37-42

Iida H, Law I, Pakkenberg B, Krarup-Hansen A, Eberl S, Holm S, Hansen AK, Gundersen HJ, Thomsen C, Svarer C, Ring P, Friberg L, Paulson OB (2000) Quantitation of regional cerebral blood flow corrected for partial volume effect using O-15 water and PET: I. Theory, error analysis, and stereologic comparison. J Cereb Blood Flow Metab 20: 1237-51

Iida H, Miyake Y, Hayashi T, Kudomi N, Ogawa M, Teramoto N, Kim, KM, Oka H, Hayashida K (2002) A new strategy for rapid clinical imaging of $rCMRO_2$, rCBF and rOEF using PET. J Nucl Med 43 (Suppl.): 62P

Inomata T, Fijiwara M, Iida H, Kudomi N, Miura I (2004) Neutron reduction of the small cyclotron for production of oxygen-15-1abeled gase. Intemalional Congress Series 1265: 97-100

Kim KM, Watabe H, Hayashi T, Kudomi N, Iida H (2004) Improved parametric images of blood flow and vascular volume by cluster analysis in $H_2{}^{15}O$ brain PET study. International Congress Series 1265: 79-83

Koeppe RA, Holden JE, Ip WR (1985) Performance comparison of parameter estimation techniques for the quantitation of local cerebral blood flow by dynamic positron computed tomography. J Cereb Blood Flow Metab. 5: 224-34

Kudomi N, Choi E, Watabe H, Kim KM, Shidahara M, Ogawa M, Teramoto N, Sakamoto E, Iida H (2003) Development of a GSO Detector Assembly for a Continuous Blood Sampling System IEEE TNS 50: 70-3

Kudomi N, Hayashi T, Teramoto N, Watabe H, Kawachi N, Ohta Y, Kim KM, Iida H (2005) Rapid quantitative measurement of $CMRO_2$ and CBF by dual administration of ^{15}O-labeled oxygen and water during a single PET scan-a validation study and error analysis in anesthetized monkeys. J Cereb Blood Flow Metab. 25: 1209-24.

Kudomi N, Watabe H, Hayashi T, Iida H. (2007) Separation of input function for rapid measurement of quantitative $CMRO_2$ and CBF in a single PET scan with a dual tracer administration method. Phys Med Biol. 52: 1893-908.

Kudomi N, Hayashi T, Watabe H, Teramoto N, Piao R, Ose T, Koshino K, Ohta Y, Iida H. (2009) A physiologic model for recirculation water correction in CMRO2 assessment with 15O2 inhalation PET. J Cereb Blood Flow Metab. 29: 355-64

Kudomi N, Watabe H, Hayashi T, Oka H, Miyake Y, Iida H (2010) Optimization of transmission scan duration for ^{15}O PET study with sequential dual tracer administration using N-index. Ann Nucl Med, 24: 413-20

Lees KR, Bluhmki E, von Kummer R, Brott TG, Toni D, Grotta JC, Albers GW, Kaste M, Marler JR, Hamilton SA, Tilley BC, Davis SM, Donnan GA, Hacke W; ECASS, ATLANTIS, NINDS and EPITHET rt-PA Study Group, Allen K, Mau J, Meier D, del Zoppo G, De Silva DA, Butcher KS, Parsons MW, Barber PA, Levi C, Bladin C, Byrnes G. (2010) Time to treatment with intravenous alteplase and outcome in stroke: an updated pooled analysis of ECASS, ATLANTIS, NINDS, and EPITHET trials. Lancet. 375: 1695-1703.

Lammertsma AA, Heather JD, Jones T, Frackowiak RS, Lenzi GL (1982) A statistical study of the steady state technique for measuring regional

cerebral blood flow and oxygen utilisation using ^{15}O J Comput Assist Tomogr 6: 566-73

Meyer E, Tyler JL, Thompson CJ, Redies C, Diksic M, Hakim AM (1987) Estimation of cerebral oxygen utilization rate by single-bolus $^{15}O_2$ inhalation and dynamic positron emission tomography. J Cereb Blood Flow Metab 7: 403-14

Mintun MA, Raichle ME, Martin WR, Herscovitch P (1984) J. Nucl., Med 25:177-87

Mintun MA, Lundstrom BN, Snyder AZ, Vlassenko AG, Shulman GL, Raichle ME (2001) Blood flow and oxygen delivery to human brain during functional activity: theoretical modeling and experimental data. Proc Natl Acad Sci U S A. 98: 6859-64

Miyake Y, Iida H, Hayashida K, Ishida Y, (2004) New method for the synthesis of ^{15}O-1abeled carbon monoxide and ^{15}O-1abeled dioxide for rapid supply in clinical use. Intemalional Congress Series 1265: 93-96

Ohta S., Meyer E., Thompson C.J., and Gjedde A (1992) J Cereb. Blood Flow Metab. 12: 175-92

Ohta S, Reutens DC, Gjedde A (1999) Brief vibrotactile stimulation does not increase cortical oxygen consumption when measured by single inhalation of positron emitting oxygen. J Cereb Blood Flow Metab 19: 260-5.

Shao L, Karp JS (1991) Cross-plane scattering correction-point source deconvolution in PET. IEEE Trans Med Img 10: 234-9

Shidahara M, Watabe H, Kim KM, Oka H, Sago M, Hayashi T, Miyake Y, Ishida Y, Hayashida K, Nakamura T, Iida H (2002) Evaluation of a commercial PET tomograph-based system for the quantitative assessment of rCBF, rOEF and rCMRO2 by using sequential administration of ^{15}O-labeled compounds. Ann Nucl Med. 16: 317-27

Shimosegawa E, Hatazawa J, Ibaraki M, Toyoshima H, Suzuki A (2005) Metabolic penumbra of acute brain infarction: a correlation with infarct growth. Ann Neurol 57: 495-504.

Subramanyam R, Alpert NM, Hoop B Jr, Brownell GL, Taveras JM (1978) A model for regional cerebral oxygen distribution during continuous inhalation of $^{15}O_2$, $C^{15}O$, and $C^{15}O_2$. J Nucl Med 19: 48-53

West J B, Oollery CT (1962) Uptake of oxygen-15-labelled CO_2 compared with carbon-11-labelled CO_2 in the lung. J Appl Physiol 17: 9-13

資料２

迅速ガスＰＥＴ検査にむけて

飯田秀博、久冨信之*、三宅義徳、山田直明**、森田奈緒美***

国立循環器病研究センター研究所　画像診断医学部
*国立大学法人　香川大学医学部　核医学
**国立循環器病研究センター病院　放射線部
***国立循環器病研究センター病院　放射線部核医学

Key words
PET、循環代謝イメージング、
急性期脳梗塞、^{15}O 標識酸素、定量化

Summary
^{15}O 標識酸素と PET を使った脳循環代謝量の定量検査法に関して、今までの試みと現状の課題について述べた。検査に要する時間は限りなく短時間化が望ましく、また、多くの作業項目が必要であるため省力化も重要な課題である。筆者らは、専用サイクロトロンと自動合成装置と画像解析ワークステーションの統一管理体系を構築し、限りなく迅速化かつ省力化された検査システムの実用化を目指すものである。

はじめに

^{15}O ガス PET 検査は脳虚血性疾患の病態をよく反映し、脳循環代謝諸量の情報量・情報精度において他検査に優ることから、脳血管障害疾患の重症度評価や、適切な治療法の選択において重要な役割を担う。しかしながら、^{15}O の放射線としての寿命が短い（約 2 分間の半減期）ために院内設置のサイクロトロンが必要である。また、多くのスタッフを必要とし、検査が煩雑であるなどの理由で、多数の症例に用いることは困難であった。また、測定に時間を要し被験者に長時間の安静を強いる制約から、短時間で治療方針決定を求められる急性期医療に応用されることはなかった。本稿では、過去の方法論を振り返り、^{15}O ガス PET 検査の意義と技術的課題を明らかにしつつ、脳梗塞医療に貢献するような次世代の PET 検査システムについて考察したい。

^{15}O-ガス検査の歴史

^{15}O 標識ガスを使った PET 検査は、脳をはじめ全身各組織の酸素代謝量を定量評価できる唯一の手段であるとして、黎明期からその有用性が期待されていた。1970 年代後半から 1980 年代前半にかけて脳血流量や酸素消費量の断層画像が可能になり、理化学研究所の唐沢氏によって開発されたミニサイクロトロンが医療機関での当該検査の発展に重要な貢献を果たした。1980 年半ばから 1990 年前半にかけて秋田脳研の研究チームによって、小型サイクロトロン、^{15}O 標識ガス自動合成装置、定量診断に必要な血中放射能計測装置な

どの周辺機器、さらに画像計算プログラムが整備され、我が国の ^{15}O ガス PET 検査の基盤となった。脳梗塞発症後の早期には局所脳血流量が低下するが酸素消費量が維持されて、結果として酸素摂取率が上昇する misery perfusion の病態、その後酸素消費量が低下するも血流量が上昇する laxuary perfusion の病態、さらに慢性期における matched perfusion の存在などが明らかになった。脳組織への酸素の運搬機能としての局所脳血流量（組織灌流）、および神経細胞の活動を示す直接指標である酸素消費量、これらのバランス指標としての酸素摂取率が、脳虚血性疾患の病態とリスクを適切に表しており、^{15}O ガス PET 検査の重要な特長であると考えられ現在に至っている。

^{15}O 標識ガス PET 検査では、一連の画像から機能画像に換算するプロセスが必要である。放射性薬剤の数理動態モデルに基づいて行われ、検査プロトコルは理論の前提条件を満たすように組み立てられる。Steady state 法では、$C^{15}O_2$ ガス吸入（あるいは $H_2{}^{15}O$ 静脈投与）および $^{15}O_2$ ガス吸入を定常的に行った後の『平衡時』の画像が、局所脳組織血流量（rCBF）、局所酸素代謝量（$rCMRO_2$）、および酸素摂取率（rOEF）に依存するとして、単純な計算式にて機能画像を計算する。単一スライス PET 装置でも平衡時にベッドを移動することで全脳撮像が可能であるという利点があった。しかし、種々の前提条件を満たすことは困難であり、誤差限界を指摘する報告が多くなされた。放射性ガスを一定の濃度で体内に安定投与すること、および検査中の全身生理機能が常に一定になるようにコントロールすることは現実には容易ではなく、長い検査時間と、吸入マスクの装着による呼吸状態の変化やストレスが血行動態を変化させ、計測の不安定化を来す（第 1 表）。英国ハマースミス病院で行われた健常者データでは正常者での rCBF 値が 90ml/min/100g から 30ml/min/100g 程度にまで広く分布したが(*1*)、種々の手技上の誤差だけでなく生理的な変動が反映された結果と考えられた。内部被ばくも大であり、現在の欧州の多くの PET 施設では、認めがたいレベルとされる。

その後、各国で体内での放射能濃度分布の平衡を必要としない方法が多く試みられ、1984 年にワシントン大学から提案されたボーラス投与 autoradiography (ARG 法)(*2*)に改良がくわえられ、国内で臨床利用されるようになった。各放射性ガスを吸入直後から短時間 PET 撮像を行い、一方では、時間とともに変化する動脈血液中の放射能濃度を持続モニターし、これを入力関数とする。脳全体を一度に撮像できるような広い視野を有し、かつ高い感度と計数率特性を保証する PET 装置が開発されたことでこの検査が実用的になった。動脈血中の放射能濃度を持続計測する装置(*3, 4*)、血中放射能濃度曲線が脳内放射能濃度と比べて遅延し(*5*)、かつ変形していること（dispersion）に対する補正法(*6*)や、^{15}O 酸素吸入検査における動脈血中代謝生成物（^{15}O 水）を補正する方法(*7, 8*)、などが開発され、1 時間以内に検査できるようになった。バイパス術やステント留置術、血管内外科術などの血行再建治療の適用決定の指標として有用であるとされ、また、急性期脳梗塞の病態においては、X 線 CT や MRI 撮像法ではよく

診断できないような不可逆領域の同定に有用であることが前臨床研究などで明らかになった。1991年には自動合成装置が臨床医療機器としての承認を得たものの、検査は1時間近くにおよび、検査は受け入れられ難く、検査中に一定の生理状態を確保することの困難さに加え、サイクロトロンの運転と合成・品質検定作業などにかかる人的配置の困難さから広く利用されるには至っていない。

近年、上記2法よりも検査時間を短縮化させた検査プロトコルが提案された。ひとつはモントリオール大学のSingle Step法と呼ばれる方法であり、一回の$^{15}O_2$ボーラス吸入後の動態からCBF, $CMRO_2$, CBV, OEFの画像をすべて計算するものである（第1図）。血液中の代謝生成物（$H_2{}^{15}O$）の影響が考慮されていないことによるバイアスと、画質が不十分だという評価がなされている。もうひとつの方法が国立循環器病研究センターから提案されたDual-Autoradiography(DARG)法と呼ばれる方法で、ARG法における$^{15}O_2$と$C^{15}O_2$あるいは$^{15}O_2$と$H_2{}^{15}O$の投与間隔を短縮させたことで、20分間で検査できる（第1図）。$C^{15}O$吸入スキャンを行わないでCBV画像の計算も行うことでさらに検査時間を短縮化するDBFM (spell outして下さい)法も提案されている(9)。^{15}Oガス投与はボーラスかあるいは1分間程度であり、CT搭載型のPET装置を利用すれば全体で検査時間は10分間以内にまで短縮できる可能性がある。全血液中の放射能濃度を持続モニターし、かつ動脈血液中の代謝生成物である$H_2{}^{15}O$を数理モデルで補正する手順はARG法と同様である。

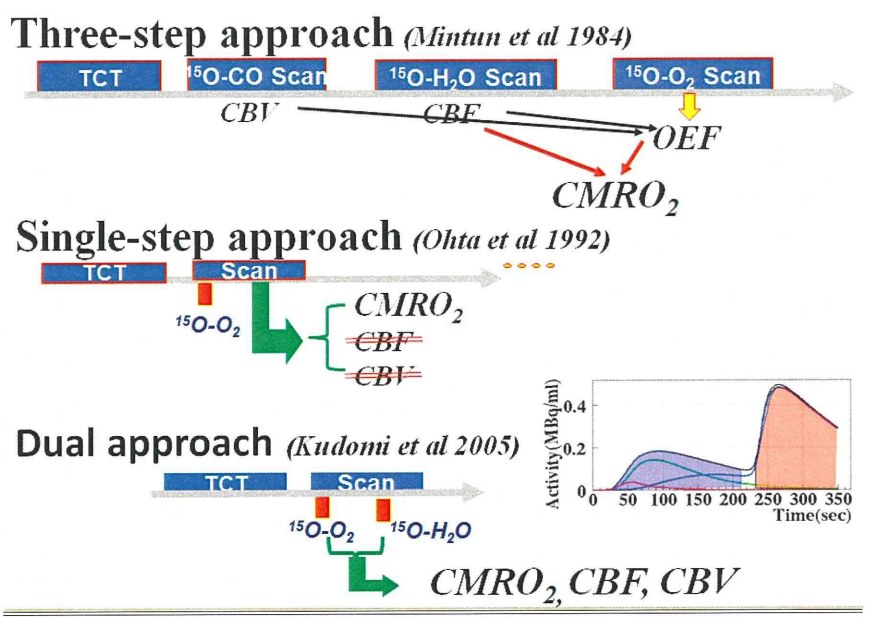

第1図　代表的な^{15}OガスPET検査プロトコルの比較。Autoradiographyに代表される3ステップ法では、3つのスキャン毎に異なる放射性薬剤が供給される。1ステップ法では$^{15}O_2$一回吸入のみで3つのパラメータを計測することを目論むが実際には$CMRO_2$のみが利用される。Dual法では、一回のスキャン中に2種の放射性ガスを吸入する。別に$C^{15}O$吸入スキャンを行うか、あるいは一回のスキャンのみでCBV画像を提示することを試みる。

定量精度と信頼性

^{15}OガスPET検査では、局所組織酸素消費量などの生理機能を定量的に計測できると言われながら、真の意味で正当性の確認がなされているわけではなかった。手技上の誤差は報告ごとに異なるため、CBF, $CMRO_2$の正常値ですら報告によって異なる（第1表）。対象群の差やガス吸入法などの違いによる真の差もあるが、撮像パラメータや解析手法の違いも少なからず影響を与える。Itohら(*10*)は国内の11施設における70名の健常者データにおいての施設間差は、手法や設定したパラメータ数値に依るものとしている。

Leendersらの報告においても、健常者のCBFや$CMRO_2$が加齢とともに減少するとしながらも、広い範囲に分散している（CBF値が90ml/min/100gから30ml/min/100g、$CMRO_2$値が2.0ml/min/100gから1.3ml/min/100g）のは、手技上の誤差の影響が大である。閉鎖式のフェースマスクが呼吸を不安定なものにし、2時間を超える検査中の変動が、結果として数値の不安定化を来していたと考えられている。^{15}Oガス吸入の安定化を図り、開放マスクの利用をもとに行われたYamaguchiらの報告ではCBFが60ml/min/100g～30ml/min/100g程度、$CMRO_2$が4.3ml/min/100g～2.3ml/min/100gに減少した。第1表に示すように、概して開放式の吸入法を採用した報告でCBFが低い傾向を認める。呼吸を安定にさせ、侵襲性を軽減する工夫と検査時間の短縮化が^{15}Oガス検査では本質的であると考えられた。

一般にPETで機能画像の定量化を行うには、数理モデルを仮定して画像計算を行う。$^{15}O_2$吸入ガスPET検査では、脳組織に移行した酸素（$^{15}O_2$）は直ちに代謝され$H_2{}^{15}O$として脳からCBFに従って洗い出される（第2図）、すなわち酸素としての血液への洗い出しは無視できるほど小さいと仮定している。この仮定は必ずしも実証されたわけではなかったが、近年筆者らの行った検討で、内頸動脈に$^{15}O_2$-標識酸化ヘモグロビンを内頸動脈にボーラス投与した後のクリアランス率が、$H_2{}^{15}O$をボーラス投与した場合とよく一致することから、本モデルの精度は十分に高いと考える。

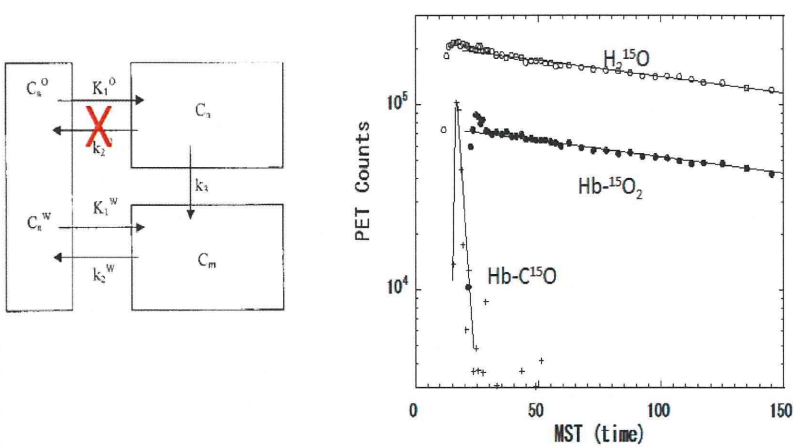

第2図　$^{15}O_2$ガスを使った局所脳酸素代謝量（$CMRO_2$）の定量計測の妥当性。脳に移行した$^{15}O_2$は直ちに代謝され$H_2{}^{15}O$としてCBFにて洗い出されると仮定している。実際に内頸動脈に$^{15}O_2$をボーラス投与した後のクリアランスは、同様に$H_2{}^{15}O$を投与した場合のクリアランスによく一致する。脳内に酸素分子として残留する分画がきわめて少ないこと、および酸素代謝量計測に利用される動態モデルの妥当性を示唆している。

第1表　過去の報告における^{15}OガスPET検査のノーマル値

報告者	方法	PET装置	CBF (min/min/100g)	CMRO2 (min/min/100g)	OEF	CBV (min/100g)	補足事項
Frackowiak RSJら (1980)	Steady state法 閉鎖式フェースマスク	CTI社 ECAT-II	65.3 ± 7.1	5.9 ± -0.59	0.49 ± 0.2	±	14名(男11, 女3)の健常者、26-74歳
Lenzi GLら (1980)	Steady state法 閉鎖式フェースマスク	CTI社 ECAT-II	64.5 ± 17.3	5.74 ± 1.12	0.49 ± 0.1	±	27名の健常者、50歳以下と以上を含む
Pantano Pら (1980)	Steady state法 閉鎖式フェースマスク	CTI社 ECAT-II	52 ± 75	5.0 ± 6.0	0.36 ± 0.5	±	2名の健常者、57歳、58歳
Yamaguchi Tら (1986)	Steady state法 開放呼吸式	島津製作所Headtome-III	42.4 ± 7.8	3.28 ± 0.45	0.44 ± 0.06	4.1 ± 0.5	灰白質領域全体、22名の健常者、26-64歳
Lammertsma AAら (1990)	持続$C^{15}O_2$吸入にARG法適用　ECAT931-08/12 閉塞式吸入	CTI社	61 ± 7	±	±	±	同日検査での再現性良好 7名の健常者、33±5歳
Leenders KLら (19890)	Steady state法 閉鎖式フェースマスク	CTI社 ECAT-II	54.5 ± 12.3	3.69 ± 0.54	0.39 ± 0.05	5.2 ± 1.4	34名(男16, 女18)の健常者、22-82歳、 insular cortex CBF:31.4-88.8ml/min/100g, CMRO:2.93-4.45 ml/min/100g, OEF: 0.27-0.50の広い範囲に分布
Hatazawa Jら (1995)	3-step ARG法 開放呼吸式	島津製作所Headtome-IV	61.5 ± 14.7	4.23 ± 0.7	0.42 ± 0.05	4.23 ± 1.04	中側頭回領域、11名の健常者、24-68歳 Delay補正が旧法でCBFなど20%過大評価
Iida Hら (2000)	3-step ARG法 開放呼吸式	島津製作所Headtome-V-Dual	39.4 ± 7.3（非採血） 40.5 5.0（動脈採血）	±	±	±	12名(男10, 女2)の健常者、22-69歳
Okazawa Hら (2001)	1-step 3WI法 開放式で吸入	GE社Advance	40.6 ± 4.6	2.19 ± 0.21	0.44 ± 0.04	2.15 ± 0.46	7名(男4, 女3)の健常者、37-55歳、 1-step 3WI法とSteady state法との比較
	Steady state法 開放式で吸入		39.8 ± 3.7	2.87 ± 0.17	0.43 ± 0.04	3.7 ± 0.48	
Hattori Nら (2004)	3-step ARG法 開放式でボーラス吸入	CTI-Siemens社 ECAT HR+ (3D収集、Neuroshield設置)	40.3 ± 5.4	2.85 ± 0.39	0.39 ± 0.06	5.3 ± 1.3	11名(男12, 女4)の健常者、35±8歳 (OEF by AV-diff:0.36±0.05)
Ibaraki Mら (2008)	3-step ARG法 閉塞式フェースマスク	島津製作所Eminence	53 ± 12	3.5 ± 0.5	0.35 ± 0.06	3.6 ± 0.3	8名の男性健常者、年齢21-24歳
Bremmer JPら (1995)	3-step ARG法 開放式で吸入	CTI-Siemens社 ECAT HR+	37.3 ± 5.5	3.03 ± 0.2	0.43 ± 0.09	2.98 ± 0.4	別日検査における再現性が良好であることを確認 10名(男6, 女4)健常者、平均69(57-80)歳
Kudomi Nら (2012a)	3-step ARG法	CTI-Siemens社 ECAT-47	51.0 ± 3.4	4.27 ± 0.43	0.41 ± 0.03	4.43 ± 0.81	
	3-step ARG法の変法 (DARG法、$H_2{}^{15}O$-$^{15}O_2$の順) 閉塞式フェースマスク		51.5 ± 3.3	4.28 ± 0.63	0.40 ± 0.04	4.43 ± 0.81	健常者(男性)7名、25.3±2.4歳
	3-step ARG法の変法 (DARG法、$^{15}O_2$-$H_2{}^{15}O$の順)フェースマスク使用		50.7 ± 3.8	4.30 ± 0.43	0.41 ± 0.04	4.43 ± 0.81	
Kudomi Nら (2012b)	迅速DBFM法 フェースマスク使用	CTI-Siemens社 ECAT-47	50.8 ± 4.0	4.21 ± 0.65	0.39 ± 0.05	5.89 ± 0.93	健常者(男性)7名、25.3±2.4歳

また、DARG 法 PET 検査をカニクイザル対象に施行したところ、PET で得た脳全体 OEF 値は内頸静脈の血中酸素分圧から求めた OEF 値と、生理的に広い範囲で一致すること（第 3 図）が確認された(*11*)。迅速化法で初めて示された事実ではあるが、Hattori らが健常者を対象に確認した報告(*12*)や、心筋領域における OEF 定量値の一致に関する報告(*13*)とあわせて、^{15}O 酸素を用いた PET 検査は、きわめて正確に $CMRO_2$ や OEF 値を計測しえることを示す。ただし、種々の手技に依存して結果が変わることについても注意が必要で、たとえば Hatazawa らの報告(*14*)では、他報告と比べて CBF 値、CMRO2 値を約 20%高く提示しているが、これは入力関数の遅延（delay）補正における誤差(*5*)で説明される。このような状況を熟知しておく必要がある。

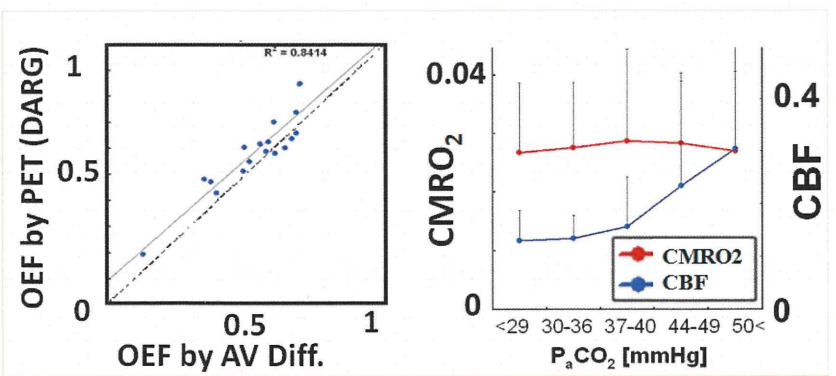

第 3 図
筆者らが行ったカニクイザルを使った妥当性評価の結果。酸素摂取率は内頸静脈採血の酸素分圧から推定した値に、生理的に広い範囲で一致しており、$PaCO_2$ に依存していない。^{15}O ガスを使って酸素消費量や酸素摂取率の絶対定量が可能であることを示す。

^{15}O ガスを用いた PET 検査で脳循環代謝量を定量評価する場合に、第 2 表に示すような種々の誤差限界がある。PET 装置の空間解像度が脳皮質構造と比べると不十分なことに起因する部分容積効果によって、CBF や $CMRO_2$ の定量値を過小評価し、その程度は PET 装置固有の空間解像度だけではなく、検査プロトコルや解析法によっても異なる。

第2表　ガスPETの誤差要因

1. 部分容積効果
   - 放射線濃度の系統的誤差
   - 動態モデルに依存した誤差伝搬
2. 入力関数の遅延と歪に対する補正誤差
   - 誤差伝搬を抑制するスキャン時間の設定が必要
3. PET装置の誤差、不安定性
   - PET装置の誤差、調整不備etc
     - ⇒散乱線補正法の改良
   - 入力関数モニター装置の誤差（感度の変動etc）
   - Wellカウンター装置の不安定さ（energy windowのズレetc）
4. 生理的変動に基づく誤差
   - 真の変動（PaCO2, Hct, Hb, etc）
   - 変動に伴う計算誤差
5. 操作エラーに基づく誤差
   - CCF操作、採血操作、撮像のタイミングetc

典型的には 50%程度の過小評価もありえるとされる(*15, 16*)が、steady state 法は ARG 法や DARG 法よりも影響が大きい。ARG 法や DARG 法では入力関数の遅延（delay）(*5*)や、これに基づく形の歪（dispersion）(*6*)が誤差要因である。動脈採血時における delay を小さくする工夫や、精度の高い補正、誤差を最小化するようなスキャン時間の選択が本質的である。視野内外に強い放射性ガスが存在することや（第 4 図）、短い検査での画像精度の確保は必ずしも容易ではなく、投与量や吸入時間、供給マスクやチューブの影響を排除する工夫も必要である。特に高感度化された 3 次元 PET (3D PET)装置ではそれらの影響もより多く受け、本質的な精度限界との競争でもある。しかし、^{15}O ガスを吸入するフェースマスクの改良や投与量の最適化、画像再構成理論の改良などにより、十分に高精度で、高解像度かつ高感度の画像が得ることが可能である（第 5 図、第 6 図）

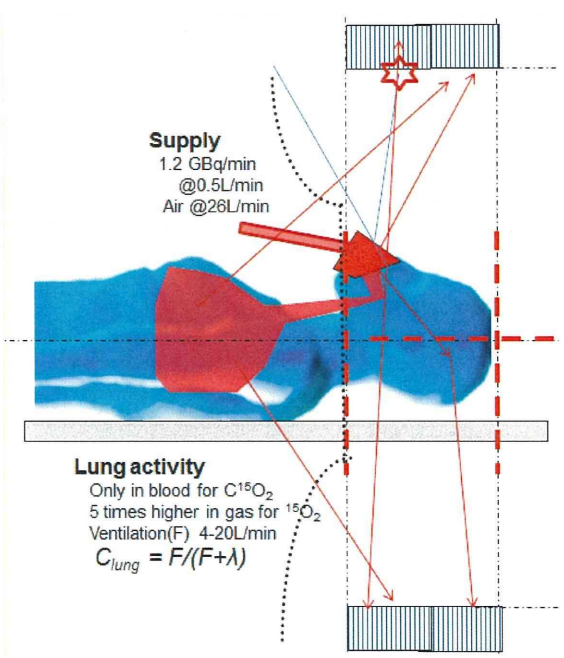

第 4 図
^{15}O ガス PET における誤差要因。吸入系における強い ^{15}O ガスの影響を排除する工夫が必要である。

空間解像度や画像精度は従来装置と比べて大きく改善した。PET 画像から血中放射能濃度の計測を行うことも可能になり、無採血定量の可能性が広がった。^{15}O ガス PET 検査の新しい応用領域の開拓に貢献するような今後の研究が期待されるところである。種々の検査手順の簡便化と標準化や、被験者に対する負担の軽減や、生理的変動を最小にする工夫も重要である。

第 5 図　最新の高感度化された 3D PET 装置で撮像した、$C^{15}O$, $^{15}O_2$, $C^{15}O_2$ 吸入中の健常者頭部のＭＩＰ画像。偶発同時計数、数え落とし、散乱線補正、を正しく補正する物理プロセスを組み込むことで、高感度、高空間解像度、高精度な計測が可能になった。頸動脈などの放射能濃度をモニタするなどの方法を用いることで無採血定量化の可能性が期待される。

技術的課題

^{15}O ガス PET 検査を実際の臨床で実施するには PET 撮像と周辺機器の操作だけでなく、動脈採血と血液データの解析、サイクロトロンの運転、一連の ^{15}O ガスの標識合成、さらに標識合成ごとに QC（安全性試験、純度検定など）などを担当するスタッフの確保が必要である。検査枠の調整は一般には容易ではなく、急性期脳梗塞疾患の検査への対応は困難であった。筆者らは、オンデマンドでも実施しえる ^{15}O ガス PET 検査システムの実用化を目指して技術整備を行ってきた。^{15}O 標識ガス合成装置においては標識合成と品質検定を迅速かつ簡便に実施できるよ

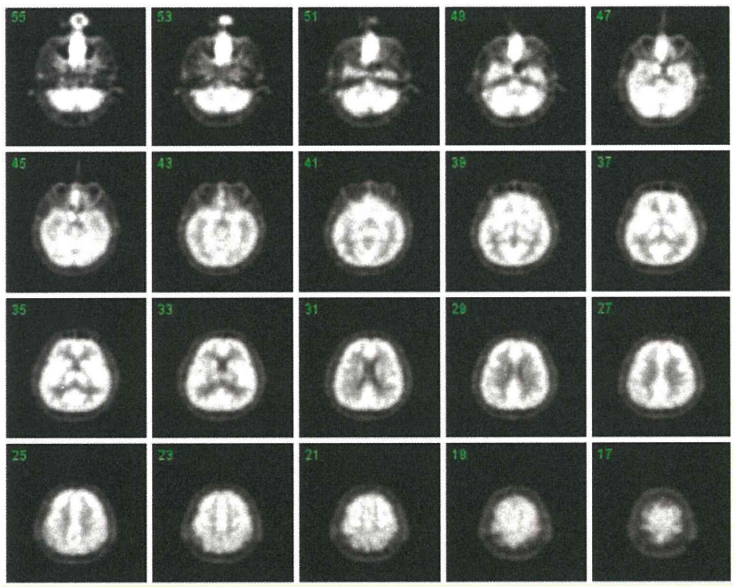

第 6 図　上記 3D PET を使って得た健常者の酸素代謝量（定性）画像の例。白質、静脈洞などの分離が鮮明である。

うな迅速検査対応型の ^{15}O ガス合成システムの開発に成功し、現在 4.5 分間隔で異なる ^{15}O 標識ガスを繰り返し供給することが可能になった。すなわち $C^{15}O$ ガス吸入を必要とする DARG 法検査でも全体で 20 分間程度、$C^{15}O$ ガス吸入を必要としない DBFM 法検査では 8～9 分間程度で一連の検査を完結させることができる。本 ^{15}O ガス合成・供給装置については、それぞれの放射性ガスを合成、供給終了した後に強制的に排気し、次の標識合成に必要なターゲットガスの充てんを迅速に行う機構を有することが特長であり、医療機器としての装置製造がなされている。さらに ^{15}O ガス専用の超型